Manuscript submitted to **Biophysical***Journal*
**Article**

# Fast adaptation of cooperative channels engenders Hopf bifurcations in auditory hair cells

Francesco Gianoli[1], Brenna Hogan[1], Émilien Dilly[2], Thomas Risler[2,*], and Andrei S. Kozlov[1,*]

[1]Department of Bioengineering, Imperial College London, London SW7 2AZ, United Kingdom
[2]Institut Curie, Université PSL, Sorbonne Université, CNRS UMR168, Laboratoire Physico-Chimie Curie, 75005 Paris, France
[*]Correspondence: a.kozlov@imperial.ac.uk or thomas.risler@curie.fr

ABSTRACT Since the pioneering work of Thomas Gold published in 1948, it has been known that we owe our sensitive sense of hearing to a process in the inner ear that can amplify incident sounds on a cycle-by-cycle basis. Termed the active process, it uses energy to counteract the viscous dissipation associated with sound-evoked vibrations of the ear's mechanotransduction apparatus. Despite its importance, the mechanism of the active process and the proximate source of energy that powers it have remained elusive—especially at the high frequencies characteristic of amniote hearing. This is partly due to insufficient understanding of the mechanotransduction process in hair cells, the sensory receptors and amplifiers of the inner ear. It has previously been proposed that a cyclical binding of $Ca^{2+}$ ions to individual mechanotransduction channels could power the active process. That model, however, relied on tailored reaction rates that structurally forced the direction of the cycle. Here, we ground our study on our previous model of hair-cell mechanotransduction, which relied on the cooperative gating of pairs of channels, and incorporate into it the cyclical binding of $Ca^{2+}$ ions. With a single binding site per channel and reaction rates drawn from thermodynamic principles, the current model shows that hair cells behave as nonlinear oscillators that exhibit Hopf bifurcations, dynamical instabilities long understood to be signatures of the active process. Using realistic parameter values, we find bifurcations at frequencies in the kilohertz range with physiological $Ca^{2+}$ concentrations. The current model relies on the electrochemical gradient of $Ca^{2+}$ as the only energy source for the active process and on the relative motion of cooperative channels within the stereociliary membrane as the sole mechanical driver. Equipped with these two mechanisms, a hair bundle proves capable of operating at frequencies in the kilohertz range, characteristic of amniote hearing.

SIGNIFICANCE How the inner ear amplifies incident sounds at frequencies of several kilohertz is a key question that has remained unanswered despite decades of research into several candidate mechanisms. Here, we model the behavior of hair cells, the sensory receptors of the inner ear, and show that they can undergo oscillatory instabilities called Hopf bifurcations due to the effect of $Ca^{2+}$ on the cooperative opening and closing of mechanotransduction ion channels. As any dynamical system close to the bifurcation point, a hair cell behaves as a nonlinear oscillator that can amplify its input on a cycle-by-cycle basis. We find that our proposed mechanism can operate in the kilohertz range.

## INTRODUCTION

The active process of the inner ear is the vibrating soul of the auditory system (1). The ear expends energy to amplify sounds, sharpen its frequency selectivity, and help compress six orders of magnitude in sound amplitude into a hundredfold range in the firing rate of the auditory fibers (2). This process is rooted in the biophysical properties of individual hair cells, the sensory receptors of the inner ear. These cells act both as microphones that pick up sound vibrations with their bundles of enlarged microvilli, called stereocilia, and as stimulus amplifiers (3). Both signal transduction and amplification rely on elastic molecular filaments, the tip links, which are connected to mechanically sensitive ion channels that open and close in unison with hair-bundle vibrations (4). Signal amplification—powered by the active process—requires a source of energy and has to be fast to operate at physiological frequencies, up to 20 kHz in humans and even higher frequencies in some other mammals.

Although the precise biophysical mechanism at the origin of the active process is still a matter of debate, the ear as a whole—as well as individual hair cells in amphibians—show signatures of dynamical systems operating close to Hopf

bifurcation points, where the system transitions from a quiescent regime to spontaneous oscillations (5, 6). Such dynamical systems display the most salient features of the active ear, including active amplification of low-intensity stimuli, sharp frequency selectivity, compressive nonlinearity in response amplitude, and spontaneous oscillations (2). Spontaneous oscillations have been proposed to underlie spontaneous otoacoustic emissions—the tones that healthy ears emit when in a quiet environment (7)—and have been measured in hair bundles of the bullfrog sacculus (8). Despite the unifying power of modeling the ear as a collection of nonlinear oscillators close to Hopf bifurcation points, the connection between the cellular and molecular biology of the inner ear and this overarching mathematical description has not yet been fully understood.

Current models of mechanotransduction reproduce well the behavior of the hair bundles of the bullfrog sacculus, which exhibit all features of the active process as they detect and amplify stimuli at frequencies on the order of tens to a hundred hertz (5, 9). These models, however, struggle to explain how auditory hair cells can achieve active amplification at frequencies in the kilohertz range, typical of mammalian hearing. This stems from the fact that such models are limited by the pace of myosin motors on which they rely to reset the working range of the hair cell on a cycle-by-cycle basis (5). Despite several pioneering studies on this subject (9–12), no microscopic model of hair-bundle motility has so far been able to reproduce the properties of active amplification at frequencies in the kilohertz range with only a minimal number of known, possible states of the channels, as well as realistic values of the gating swing—the amplitude of the conformational change of an individual channel upon opening or closing. In mammals, sparse evidence suggests that hair bundles are capable of generating forces that could drive the active process (13, 14); yet, no mammalian hair cell has ever been observed to oscillate spontaneously. The source of amplification in the cochlea has rather been attributed to electromotiliy, the ability of mammalian outer hair cells to change their length in response to changes in their transmembrane electrical potential (15). Electromotility, however, is constrained by the frequency response of prestin—the molecular driver of electromotility in outer hair cells—which is low-pass filtered with a corner frequency of a few kilohertz (16). Measurements *in vivo* indicate that this cut-off frequency lies about 2.8 octaves below the characteristic frequency of the basilar membrane at the same location, suggesting that electromotility is unlikely to be the main mechanism responsible for sound amplification on a cycle-by-cycle basis (17). Although essential for mammalian hearing, electromotility alone cannot account for all the hallmarks of the active process because it is mostly linear at small displacements (18), and because the hallmarks of the active process persist under conditions where electromotility vanishes (19). For instance, stimulus amplification in a cochlear segment could be achieved independently from the hair-cell transmembrane electrical potential, the driver of electromotility (19). Finally, birds and some species of lizards can hear sounds in the kilohertz range, yet their hair cells are devoid of prestin and do not display electromotility. If there is a parsimonious explanation for amplification—a single mechanism underlying the active process at these frequencies in all amniotes—one must look for it elsewhere.

Here, we present a new model of hair-bundle motility that relies on the electrochemical gradient of $Ca^{2+}$ as an energy source to power active oscillations, similarly to what has been proposed by Choe *et al.*, (1998) (10). We base our model on an earlier proposal that each tip link is connected to more than one mechanotransduction channels, whose states are reciprocally coupled to hair-bundle motion by elastic forces mediated by protein linkages as well as by the membrane (20). This model is not limited by the action of myosin motors, and we show here that it can produce spontaneous oscillations at frequencies of a few kilohertz, characteristic of the hearing organs of birds, some lizards, and large mammals. With two channels per tip link, the model relies on one $Ca^{2+}$ binding site per channel with transition rates derived from thermodynamic principles. Associated to the two different states of the channel pair—open-open or closed-closed—is a difference in the membrane elastic energy due to different membrane deformations to match the different thicknesses of the hydrophobic region of each channel in its open and closed states (20, 21). As a result, the model produces spontaneous oscillations with no requirement for a large individual-channel gating swing, as long as the hydrophobic region of the channel has different thicknesses in the open and closed states. We describe the details of this model in the next section.

## MODEL

Based on previous work (20), we hypothesize that in a mature hair bundle every tip link is connected to two functional mechanosensitive ion channels (22, 23). These channels are mobile in the membrane and they each connect to one of the two strands of the tip link at its lower end (24). Two adaptation springs anchor the channels to the cytoskeleton (see Fig. 1 and Fig. 2A). Although initially a conjecture (20), this connection has later been confirmed experimentally in *Caenorhabditis elegans* for transmembrane channel-like proteins (TMC) (25), which are molecular components of hair-cell mechanotransduction channels (26–28). The two channels function as a unit due to a reciprocal coupling between their conformational states (open or closed) and the local thickness of the membrane (21, 29, 30). This reciprocal coupling stems from the different hydrophobic regions of the channel in the open and closed states, causing a state-dependent hydrophobic mismatch with the lipid bilayer around the channel and therefore deforming it differently in these two states (21, 30). Minimizing the energy, which includes the elastic energy of the membrane surrounding the channels, results in cooperative gating, such that only two gating

states (open-open (OO) and closed-closed (CC)) are effectively at play for the pair. In contrast to the classical gating-spring model (4, 31), the observed relaxation of the hair bundle upon channel opening is provided by the motion of the channels in the membrane plane rather than by the individual-channel gating swing.

Here, we add to that description an active process that is based on a cycle of $Ca^{2+}$ binding and unbinding to the channels, similarly to what was proposed by Choe *et al.* (10) in 1998. We hypothesize that the binding of one $Ca^{2+}$ ion to a channel lowers the energy of the closed state, while leaving the open state unaffected. Given that $Ca^{2+}$ binding is a diffusion-limited process, the rate of $Ca^{2+}$ binding is proportional to its local concentration, whereas that of $Ca^{2+}$ unbinding does not depend on it. Since $Ca^{2+}$ diffusion over several nanometers occurs on much shorter timescales than those of interest here, we estimate that the $Ca^{2+}$ concentration at the channel's binding site equilibrates instantaneously to two values, one for each channel state (open or closed). We therefore introduce two rates of $Ca^{2+}$ binding, thereby breaking thermodynamic equilibrium. We show that such an active process is able to drive spontaneous oscillations of the hair bundle (Fig. 1). In response to a change of parameter values, and notably of $Ca^{2+}$ concentration in the vicinity of the open channel, the hair bundle transitions between a quiescent and an oscillatory regimes. This transition corresponds to a Hopf bifurcation, where the system's sensitivity is maximal.

## Force balance

This part of the model is identical to the model published in (20). Force balance on the hair bundle reads:

$$M_{\mathrm{HB}}\ddot{X} = -\xi_{\mathrm{HB}}\dot{X} - K_{\mathrm{sp}}(X - X_{\mathrm{sp}}) - \gamma \sum_{j=1}^{N_{\mathrm{t}}} f_{\mathrm{t}}^{j} \,. \tag{1}$$

Here, $X$ denotes the position of the tip of the hair bundle, projected onto the direction of mechanosensitivity, $\dot{X}$ and $\ddot{X}$ are its first and second time derivatives, and $X_{\mathrm{sp}}$ is the resting position of the hair bundle in the absence of tip links, due to the action of the stereociliary pivots; $M_{\mathrm{HB}}$ is the hair bundle's apparent wet mass (32) (see section Parameter values), $\xi_{\mathrm{HB}}$ the bundle's viscous drag coefficient, $K_{\mathrm{sp}}$ the combined stiffness of the stereociliary pivots, and $N_{\mathrm{t}}$ the number of tip links. The scaling factor $\gamma$ is the approximately constant projection factor of the tip-link axis on the hair-bundle displacement axis, such that for a change of position of the hair bundle $X$, the tip-link extension changes by $x = \gamma X$. Each of the $N_{\mathrm{t}}$ tip links in the hair bundle contributes a projected force $f_{\mathrm{t}}^{j}$ along the tip-link axis given by

$$f_{\mathrm{t}}^{j} = k_{\mathrm{t}}(\gamma(X - \tilde{X}_0) - d^{j}) \,, \tag{2}$$

where $k_{\mathrm{t}}$ is the tip-link stiffness and $d^{j}$ the varying distance between the tip-link fork and the membrane of the lower stereocilium along the tip-link axis. An illustration of the corresponding geometry is shown in Fig. 2A. The displacement $\tilde{X}_0$ is a reference position of the $X$-axis that sets a reference tension in the tip links for a given hair-bundle position $X$ and distance $d$. This tension stems from the action of myosin motors, which incessantly pull on the tip link's upper insertion point (33). The parameter $\tilde{X}_0$ is therefore linked to a reference position of these myosin motors. Focusing on shorter timescales than those associated with myosin-motor displacements, we consider $\tilde{X}_0$ as a constant quantity in the following.

To close the system of equations, we now need to determine how the distance $d^{j}$ relates to the hair-bundle displacement $X$, for each tip link $j$. Force balance on either of the two channels connected to the tip link reads:

$$k_{\mathrm{t}}(\gamma(X - \tilde{X}_0) - d) = 2\frac{d + a\sin\alpha}{a + d\sin\alpha}\left[k_{\mathrm{a}}\left(a_{\mathrm{adapt}} - a - \frac{n}{2}\delta\right) - \frac{dV_{\mathrm{b},n}}{da}\right] , \tag{3}$$

where the coordinate $a$ corresponds to the distance between either of the two anchoring points of the tip link and the tip link's central axis, $\alpha$ is the angle between the perpendicular to the tip-link axis and the membrane plane, $k_{\mathrm{a}}$ is the adaptation springs' stiffness, $a_{\mathrm{adapt}}$ sets the inter-channel distance for which the adaptation springs slacken, $\delta$ is the single-channel gating swing, $n = 0$, 1, or 2 is the number of open channels in the pair, and $V_{\mathrm{b},n}$ is the elastic potential of the lipid bilayer in which the mechanosensitive channels are embedded, which depends on $n$ (see Fig. 2A). This elastic membrane potential is derived from the one-dimensional interaction potentials mediated by the membrane between two mechanosensitive channels of large conductance (MscL) in *Escherichia coli*, as modeled by Ursell *et al.* (21, 30). Following our previous study (20), we mimic the

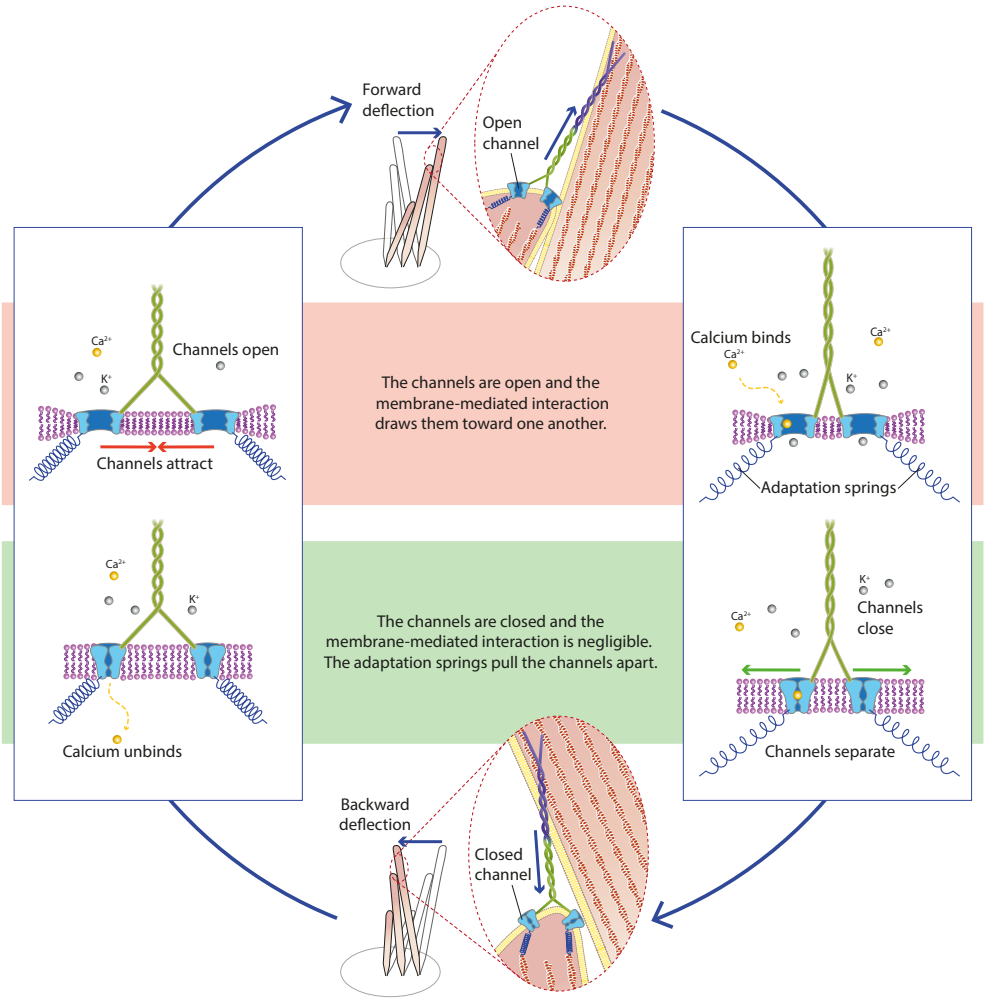


Figure 1: Schematics of the hair-bundle oscillations driven by $Ca^{2+}$ binding and unbinding (bundle deflections are exaggerated for the purpose of the illustration). We start the description of the cycle from the left box, upper drawing, with both channels open and no $Ca^{2+}$ bound. In that configuration, the membrane-mediated interaction between the two channels drives them toward one another (left box, upper panel, red arrows). This movement relaxes tension in the tip link, therefore allowing the stereociliary pivots to drive the hair bundle to the right (top illustration, blue arrows). The channels being open, $Ca^{2+}$ enters and subsequently binds to one of the two channels, facilitating its closure. Since the open-closed state is strongly disfavored energetically due to the membrane-mediated interaction between the channels, this triggers the closure of the second channel almost simultaneously (right box, lower panel). In this closed-closed configuration, the membrane's elastic potential is almost flat and tension in the adaptation springs pulls the channels apart (green arrows). The resulting increase of tension in the tip link causes the bundle to twitch backwards (bottom illustration, blue arrows). Now that the channels are closed, the intracellular $Ca^{2+}$ concentration at the binding sites decreases, which lowers their occupancy (left box, lower panel). Tension in the springs then tends to reopen the channels, thus bringing us back to where we started and completing the cycle of oscillations. At steady state, a thermodynamic equilibrium exists between the open-open state with the channels closer to one another and the closed-closed state with the channels farther apart.

shape of the elastic potentials used in that study with the following analytic expressions:

$$\begin{aligned} V_{\mathrm{b},0}(a) &= E_{\mathrm{CC}}\left(\frac{a-a_{\mathrm{cross,CC}}}{a_{\mathrm{min}}-a_{\mathrm{cross,CC}}}\right)\exp\left[-\left(\frac{a-a_{\mathrm{min}}}{l_{\mathrm{v}}}\right)^2\right] \\ V_{\mathrm{b},1}(a) &= E_{\mathrm{OC}}\left[\frac{(a_{\mathrm{cross,OC}}-a)(a_{\mathrm{cross,OC}}-a_{\mathrm{min}})^2}{(a-a_{\mathrm{min}})^3}\right]\exp\left[-\left(\frac{a-a_{\mathrm{min}}}{l_{\mathrm{v}}}\right)^2\right] \\ V_{\mathrm{b},2}(a) &= E_{\mathrm{OO}}\left(\frac{a-a_{\mathrm{cross,OO}}}{a_{\mathrm{min}}-a_{\mathrm{cross,OO}}}\right)\exp\left[-\left(\frac{a-a_{\mathrm{min}}}{l_{\mathrm{v}}}\right)^2\right]. \end{aligned} \tag{4}$$

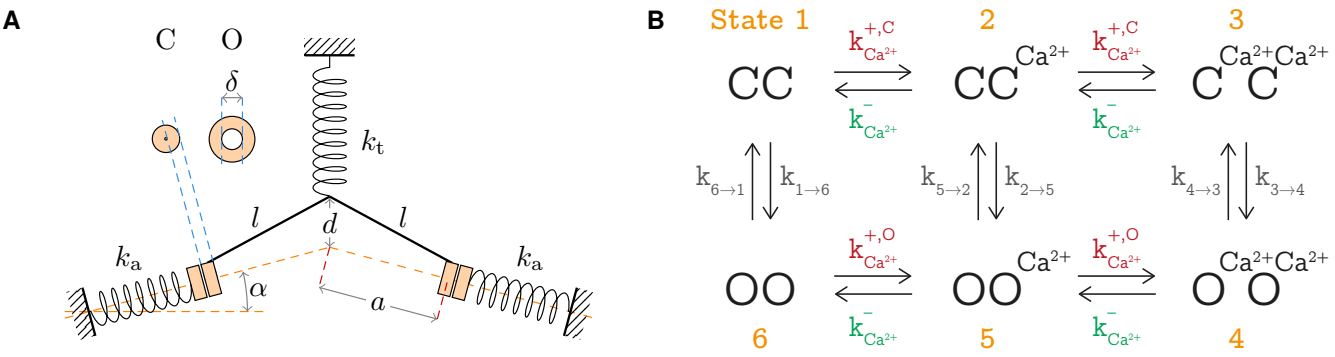


Figure 2: (A) Geometry of the two-channel model and associated parameters. The orange annuli represent the mechanosensitive channel in the closed (C) and open (O) configurations, seen orthogonally to the membrane plane. The system of springs is shown in the CC configuration. (B) Schematic representation of the six different states considered for a channel pair. States 1, 2, and 3 correspond to both channels closed, with respectively either zero, one, or two calcium ions bound. States 4, 5, and 6 correspond to both channels open, similarly with different numbers of calcium ions. Each allowed direct transition is characterized by a rate constant, where the transitions $1 \rightleftharpoons 6$, $2 \rightleftharpoons 5$, and $3 \rightleftharpoons 4$ correspond to opening or closing of the channels, and $1 \rightleftharpoons 2$, $2 \rightleftharpoons 3$, $4 \rightleftharpoons 5$, and $5 \rightleftharpoons 6$ correspond to binding or unbinding of one $Ca^{2+}$.

The values of the different parameters entering these expressions are given in Table 1, and a plot is provided in (20). Finally, geometrical constraints impose that $d$ and $a$ are related by:

$$d = \sqrt{l^2 - (a\cos\alpha)^2} - a\sin\alpha\,, \tag{5}$$

where $l$ is the length of the tip-link fork. A full description of that part of the model together with detailed graphical illustrations is given in (20), and additional parameter values used here are all provided in Table 1.

## Calcium cycle

We describe here the implementation of the influence of $Ca^{2+}$ binding and unbinding to the channels on their gating states. We hypothesize one $Ca^{2+}$ binding site per channel, which leads to a total of three $Ca^{2+}$-binding states for a given pair of channels, with a total of either zero, one, or two ions bound to the pair. As argued above, the rates of $Ca^{2+}$ binding are proportional to the local $Ca^{2+}$ concentration, $[Ca^{2+}]^{\text{open}}$ and $[Ca^{2+}]^{\text{closed}}$ in the open and closed states, respectively. The rate of $Ca^{2+}$ unbinding, however, is independent of the local concentration and therefore independent of the channels' state in our model. Together, this leads to:

$$\begin{aligned} k^{+,O}_{Ca} &= k_b[Ca^{2+}]^{\text{open}} \\ k^{+,C}_{Ca} &= k_b[Ca^{2+}]^{\text{closed}} \\ k^{-}_{Ca} &= k_b K_d\,, \end{aligned} \tag{6}$$

where $k^{+,O}_{Ca}$ and $k^{+,C}_{Ca}$ are the rates of $Ca^{2+}$ binding in the open and closed states, respectively, $k^{-}_{Ca}$ is the rate of $Ca^{2+}$ unbinding, $k_b$ is the reaction constant of $Ca^{2+}$ binding, and $K_d$ is the $Ca^{2+}$ dissociation constant.

## Opening and closing transition rates

To complete the model, we now focus on identifying the probabilities of the different states that a channel pair can occupy, and how they evolve in time. With physiological parameters, and taking into account the membrane elastic potentials, the energy of the open-closed (OC) state is higher than that of either OO or CC states. In the following, we therefore ignore the occupancy of this state and investigate only the transitions between the OO and CC states. This corresponds to investigating a perfect cooperativity between the two channels, mediated by the lipid bilayer (20). Taking into account the different occupancy states of the channels by $Ca^{2+}$, we are therefore left with a total of six states: three $Ca^{2+}$ binding states for each of the two gating states of the channel pair.

Transitions between each of these adjacent states in this calcium cycle occur with specific rates, schematically represented in Fig. 2B. Among these rates, the $Ca^{2+}$ binding and unbinding rates have already been discussed, and we need to specify

the transition rates between the OO and CC states with a given number of bound $Ca^{2+}$ ions. To write these rates, we suppose that each of these transitions goes through its respective OC state, which serves as a limiting transition state. The associated activation energy allows to write the transition rate using Kramers' reaction-rate theory. We hypothesize that the presence of one calcium ion bound to a closed channel lowers its energy by the fixed amount $E_{\mathrm{Ca}}$. The energies of each of the six states represented in Fig. 2 therefore read:

$$\begin{cases} E_1 = E_{\mathrm{CC}} \\ E_2 = E_{\mathrm{CC}} - E_{\mathrm{Ca}} \\ E_3 = E_{\mathrm{CC}} - 2E_{\mathrm{Ca}} \\ E_4 = E_5 = E_6 = E_{\mathrm{OO}}\,, \end{cases} \tag{7}$$

where $E_{\mathrm{CC}}$ and $E_{\mathrm{OO}}$ are respectively the energies of the CC and OO states in the absence of calcium ions. The energies $E_{1\rightleftharpoons 6}$, $E_{2\rightleftharpoons 5}$, and $E_{3\rightleftharpoons 4}$ of the respective transition states between states 1 and 6, 2 and 5, and 3 and 4, in both directions, read:

$$\begin{cases} E_{1\rightleftharpoons 6} = E_{\mathrm{OC}} \\ E_{2\rightleftharpoons 5} = E_{\mathrm{OC}} - E_{\mathrm{Ca}} \\ E_{3\rightleftharpoons 4} = E_{\mathrm{OC}} - E_{\mathrm{Ca}}\,. \end{cases} \tag{8}$$

For the transition state between states 2 and 5, there are *a priori* two possibilities: OCa–C and O–CCa. As we know that the closed state is stabilized by calcium, the intermediate state O–CCa is of lower energy. Due to the exponential dependence of the transition rate on the transition-state energy, we consider that the state O–CCa is strongly favored, leading to the expression given above. Note that we assume that the binding of $Ca^{2+}$ does not affect the energy of the open state. As a result, the height of the energy barrier in the transitions $5 \to 2$ and $4 \to 3$ is lowered by $E_{\mathrm{Ca}}$ in both cases as compared with that of the transition $6 \to 1$. The energy barriers in the opposite directions, however, behave differently: the barrier of the transition $2 \to 5$ is unchanged as compared to that of $1 \to 6$, and that of $3 \to 4$ is increased by $E_{\mathrm{Ca}}$. Given these energies, Kramers' rate theory allows us to write the following expressions for the forward and reverse transition rates between states 1 and 6, 2 and 5, and 3 and 4:

$$\begin{cases} k_{1\to 6} = \bar{k}\, \mathrm{e}^{-\beta(E_{\mathrm{OC}} - E_{\mathrm{CC}})} \\ k_{6\to 1} = \bar{k}\, \mathrm{e}^{-\beta(E_{\mathrm{OC}} - E_{\mathrm{OO}})} \\ k_{2\to 5} = \bar{k}\, \mathrm{e}^{-\beta(E_{\mathrm{OC}} - E_{\mathrm{CC}})} \\ k_{5\to 2} = \bar{k}\, \mathrm{e}^{-\beta(E_{\mathrm{OC}} - E_{\mathrm{OO}} - E_{\mathrm{Ca}})} \\ k_{3\to 4} = \bar{k}\, \mathrm{e}^{-\beta(E_{\mathrm{OC}} - E_{\mathrm{CC}} + E_{\mathrm{Ca}})} \\ k_{4\to 3} = \bar{k}\, \mathrm{e}^{-\beta(E_{\mathrm{OC}} - E_{\mathrm{OO}} - E_{\mathrm{Ca}})}\,, \end{cases} \tag{9}$$

where $\beta = 1/(k_{\mathrm{B}}T)$ is the thermodynamic *beta* or inverse thermal energy, with $k_{\mathrm{B}}$ the Boltzmann constant and $T$ the temperature, and where $\bar{k}$ is a pre-exponential factor called 'the attempt frequency' that sets a baseline rate to these transitions.

## Probability dynamics

We can now write the time-evolution equations for the occupancy probabilities of each of the six different states shown in Fig. 2:

$$\begin{cases} \dot{p_1} = 2k_{\mathrm{Ca}}^{-} e^{-\beta E_{\mathrm{Ca}}} p_2 + \bar{k} e^{-\beta(E_{\mathrm{OC}} - E_{\mathrm{OO}})} p_6 - \left[ \bar{k} e^{-\beta(E_{\mathrm{OC}} - E_{\mathrm{CC}})} + k_{\mathrm{Ca}}^{+,\mathrm{C}} e^{\beta E_{\mathrm{Ca}}} \right] p_1 \\ \dot{p_2} = \bar{k} e^{-\beta(E_{\mathrm{OC}} - E_{\mathrm{OO}} - E_{\mathrm{Ca}})} p_5 + \frac{1}{2} k_{\mathrm{Ca}}^{-} e^{-\beta E_{\mathrm{Ca}}} p_3 + \frac{1}{2} k_{\mathrm{Ca}}^{+,\mathrm{C}} e^{\beta E_{\mathrm{Ca}}} p_1 - \left[ \bar{k} e^{-\beta(E_{\mathrm{OC}} - E_{\mathrm{CC}})} + k_{\mathrm{Ca}}^{+,\mathrm{C}} e^{\beta E_{\mathrm{Ca}}} + k_{\mathrm{Ca}}^{-} e^{-\beta E_{\mathrm{Ca}}} \right] p_2 \\ \dot{p_3} = 2k_{\mathrm{Ca}}^{+,\mathrm{C}} e^{\beta E_{\mathrm{Ca}}} p_2 + \bar{k} e^{-\beta(E_{\mathrm{OC}} - E_{\mathrm{OO}} - E_{\mathrm{Ca}})} p_4 - \left[ \bar{k} e^{-\beta(E_{\mathrm{OC}} - E_{\mathrm{CC}} + E_{\mathrm{Ca}})} + k_{\mathrm{Ca}}^{-} e^{-\beta E_{\mathrm{Ca}}} \right] p_3 \\ \dot{p_4} = 2k_{\mathrm{Ca}}^{+,\mathrm{O}} p_5 + \bar{k} e^{-\beta(E_{\mathrm{OC}} - E_{\mathrm{CC}} + E_{\mathrm{Ca}})} p_3 - \left[ \bar{k} e^{-\beta(E_{\mathrm{OC}} - E_{\mathrm{OO}} - E_{\mathrm{Ca}})} + k_{\mathrm{Ca}}^{-} \right] p_4 \\ \dot{p_5} = \frac{1}{2} k_{\mathrm{Ca}}^{+,\mathrm{O}} p_6 + \frac{1}{2} k_{\mathrm{Ca}}^{-} p_4 + \bar{k} e^{-\beta(E_{\mathrm{OC}} - E_{\mathrm{CC}})} p_2 - \left[ k_{\mathrm{Ca}}^{-} + k_{\mathrm{Ca}}^{+,\mathrm{O}} + \bar{k} e^{-\beta(E_{\mathrm{OC}} - E_{\mathrm{OO}} - E_{\mathrm{Ca}})} \right] p_5 \\ \dot{p_6} = 2k_{\mathrm{Ca}}^{-} p_5 + \bar{k} e^{-\beta(E_{\mathrm{OC}} - E_{\mathrm{CC}})} p_1 - \left[ \bar{k} e^{-\beta(E_{\mathrm{OC}} - E_{\mathrm{OO}})} + k_{\mathrm{Ca}}^{+,\mathrm{O}} \right] p_6\,. \end{cases} \tag{10}$$

Note that the prefactors 2 and $1/2$ that appear in some terms are due to the fact that the states 2 and 5 are degenerate: in both instances, a single $Ca^{2+}$ ion is free to bind to either of the two available channels, with the same resultant energy in either case.

## Expression of the energies

In the system of equations 10, the energies $E_{\mathrm{OO}}$, $E_{\mathrm{OC}}$, and $E_{\mathrm{CC}}$ correspond to the energies of one pair of channels in the respective configurations. These energies include the elastic contributions from the extensions of the tip link and adaptation springs, that of the lipid-bilayer deformations $V_{\mathrm{b},n}$, as well as the gating energy of the channels $E_{\mathrm{g}}$, the energy difference between the open and closed states of a single channel. We define the following energy function for a pair of $n = 0$, 1, or 2 open channels, located a distance $2a$ apart, the hair bundle being positioned at $X$:

$$E(a,X,n) = 2\times\frac{k_{\mathrm{a}}}{2}\left(a_{\mathrm{adapt}}-a-\frac{n}{2}\delta\right)^2\Theta\left(a_{\mathrm{adapt}}-a-\frac{n}{2}\delta\right)+\frac{k_{\mathrm{t}}}{2}(\gamma(X-\tilde{X}_0)-d)^2\,\Theta\left(\gamma(X-\tilde{X}_0)-d\right)+V_{\mathrm{b},n}(a)+nE_{\mathrm{g}}\,. \quad (11)$$

Here, $d$ is a function of the half inter-channel distance $a$ thanks to the geometric relation 5, and $\Theta$ is the Heaviside step function that represents slacking, since neither the tip links nor the adaptation springs are supposed to resist compression. The energies $E_{\mathrm{OO}}$, $E_{\mathrm{OC}}$, and $E_{\mathrm{CC}}$ in Eq. 10 equal $E(a,X,n)$ as given in Eq. 11 with $n = 0$, 1, or 2, respectively.

As seen in Eq. 3, together with Eq. 5, the position of the hair bundle's tip $X$ is a function of the half inter-channel distance $a$ as well as of the number $n$ of open channels in the pair via the elastic membrane potential $V_{\mathrm{b},n}$. We therefore have three different relations $X(a)$—one per gating state of the pair (OO, OC, or CC). Each of these relations is invertible, such that we can write the equations in terms of the sole variable $X$, replacing the variable $a$ in state $n$ in Eq. 11 by the corresponding solution to Eq. 3, $a_n(X)$. Finally, we obtain expressions that can be summarized under the form:

$$\begin{cases} E_{\mathrm{CC}}(X) = E(a_0(X),X,0) \\ E_{\mathrm{OC}}(X) = E(a_1(X),X,1) \\ E_{\mathrm{OO}}(X) = E(a_2(X),X,2)\,. \end{cases} \quad (12)$$

## Closing the system

Considering that Eq. 1 is second order, we can split it into two first-order equations by introducing the variable $Y = \dot{X}$. Doing so, we use the vector $\mathbf{S} = (X, Y, p_1, p_2, p_3, p_4, p_5, p_6)^{\mathrm{T}}$ to represent the state of the system at any given time, where the symbol 'T' corresponds to the matrix transposition operation. The whole model now reads:

$$\dot{\mathbf{S}} = \mathbf{F}(\mathbf{S})\,, \quad (13)$$

where the vectorial function $\mathbf{F}$ corresponds to Eqs. 1 and 10, together with the other equations given above that allow to express $\mathbf{F}$ as a function of the components of $\mathbf{S}$ only.

## Parameter values

Several of the model parameters can be estimated from the literature. We list in Table 1 the parameters that relate to the mechanics of the hair bundle, that of the elastic deformations of the membrane, and to the calcium cycle. The parameters that do not appear in Table 1 are the same as the default values in ref. (20). The parameter $\tilde{X}_0$ entering Eq. 2 is not directly observable from experiments, as it is linked to the position of myosin motors within stereocilia. To infer its value, we first choose that the origin of the $X$ axis ($X = 0$) is such that it is a resting point of the hair bundle, i.e. a static solution of Eq. 1. This fixes the value of $X_{\mathrm{sp}}$, the resting position of the stereociliary pivots relative to the origin, provided that we know all the other parameters in that equation. To determine the value of $\tilde{X}_0$, we impose in addition that, at $X = 0$, the steady-state open probability of the channels $P_{\mathrm{open}} = p_4 + 2p_5 + p_6$ equals 0.15. This value corresponds to the resting open probability of mammalian inner hair cells tuned to kilohertz frequencies (36–39).

The parameter $M_{\mathrm{HB}}$ represents the effective mass of the hair bundle as it moves in liquid. The total mass of stereocilia in a hair bundle can be estimated from the bundle's geometry and the actin content of stereocilia. This leads to a 'dry mass' of about 50–60 pg (8, 40). However, hair bundles are immersed in liquid. As they oscillate, they drag along an additional volume of fluid located within the boundary layer, effectively increasing the apparent hair bundle's mass (41). Such a 'wet mass' has been estimated using a detailed finite-element model of the hair bundle and its surrounding fluid to be on the order of 100 pg (32).

## RESULTS

Having all parameters at hand, we perform linear-stability analysis around the fixed point $X = 0$ on the dynamics given by Eq. 13. In the following figures, we plot the real and imaginary components of the pair of eigenvalues with maximum real part, which characterize the dynamics of our system in the proximity of the steady state. As this pair of complex-conjugated

Table 1: Model's parameters

| | Parameter | Description | Value | Source |
|---|---|---|---|---|
| **Mechanics** | $\alpha$ | Angle of adaptation springs with respect to horizontal | 15° | |
| | $K_{sp,0}$ | Reference combined stiffness of the stereociliary pivots | 0.65 mN·m$^{-1}$ | Jaramillo and Hudspeth (34) |
| | $\gamma_0$ | Reference geometrical scaling factor | 0.12 | Choe *et al.* (10) |
| | $N_t$ | Number of tip links | $7/8 \cdot N_s$ | Choe *et al.* (10) |
| | $M_{HB}$ | Wet mass of the hair bundle | 100 pg | Baumgart (32) |
| | $\xi_{HB}$ | Friction coefficient of the hair bundle | 100 nN·s·m$^{-1}$ | Choe *et al.* (10) |
| **Elastic membrane potentials** | $a_{min}$ | Minimal value of $a$ | 1.5 nm | |
| | $l_v$ | Characteristic decay length | 1.5 nm | |
| | $a_{cross,CC}$ | Reference value of $a$ in the CC state | 3 nm | |
| | $a_{cross,OC}$ | Reference value of $a$ in the OC state | 2.75 nm | All adapted from Ursell *et al.* (21) |
| | $a_{cross,OO}$ | Reference value of $a$ in the OO state | 2.5 nm | |
| | $E_{CC}$ | Value of $V_{b,0}$ at $a_{min}$ | -2.5 $k_BT$ | |
| | $E_{OO}$ | Value of $V_{b,2}$ at $a_{min}$ | 50 $k_BT$ | |
| **Calcium cycle** | $E_{Ca^{2+}}$ | Energy associated to $Ca^{2+}$ binding/unbinding (closed state) | 1 $k_BT$ | adapted from Beurg *et al.* (35) |
| | $k_b$ | Reaction constant of $Ca^{2+}$ binding/unbinding | 1 ms$^{-1}$·µM$^{-1}$ | Choe *et al.* (10) |
| | $\bar{k}$ | Attempt frequency for channel opening and closing | 10 ms$^{-1}$ | Beurg *et al.* (35) |
| | $K_d$ | $Ca^{2+}$ dissociation constant | 20 µM | Beurg *et al.* (35) |
| | $[Ca^{2+}]^{closed}$ | $Ca^{2+}$ concentration at the binding site of a closed channel | 0.05 µM | Choe *et al.* (10) |
| | $[Ca^{2+}]^{open}$ | $Ca^{2+}$ concentration at the binding site of an open channel | 37 µM | Choe *et al.* (10) |

eigenvalues crosses the imaginary axis, the real part changes sign and an oscillatory decay becomes a limit-cycle oscillation, corresponding to a Hopf bifurcation (6). All the other eigenvalues have negative real parts. They correspond to modes that relax on a finite timescale at the bifurcation. More generally, looking at the long-time dynamics of the hair bundle, only the pair of eigenvalues of largest real component controls its behavior.

We start by investigating the dependence of the eigenvalues on the number of stereocilia $N_s$ in the hair bundle. Along the tonotopic axis of the cochlea, hair cells tuned to higher frequencies have more stereocilia than those tuned to lower frequencies, and their stereocilia tend to be shorter, which renders their hair bundles stiffer (42–44). In addition, the total mass of actin contained in each hair bundle of a given cochlea has been shown to be roughly constant along the chicken's cochlea (45). This suggests a relationship between the geometric gain factor $\gamma$, the collective stereociliary pivot stiffness $K_{sp}$, and the number of stereocilia in the bundle $N_s$ (10). Specifically, we follow ref. (10) and assume that $\gamma \propto N_s$ and $K_{sp} \propto N_s^3$, therefore reducing the number of free parameters in the model. We postulate therefore that $K_{sp} = K_{sp,0} \cdot (N_s/50)^3$ and $\gamma = \gamma_0 \cdot (N_s/50)$, where $K_{sp,0}$ and $\gamma_0$ are a reference stiffness of the stereociliary pivots and a reference scaling factor in a hair bundle with 50 stereocilia. Their values are set to correspond to those used in (20) (see Table 1).

We investigate the dependence of the characteristic frequency of the modeled hair bundle on $N_s$, following the constant actin-mass hypothesis described above, to compare our results with those of ref. (10). We plot in Fig. 3 this dependence for three values of the attempt frequency $\bar{k}$. For small values of $\bar{k}$, the hair bundle remains quiescent, regardless of the number of stereocilia $N_s$ (Fig. 3A). For large values of $\bar{k}$, the hair bundle oscillates above a critical value of $N_s$ (Fig. 3C). At intermediate values of $\bar{k}$, the hair bundle oscillates within a limited range of $N_s$ values (Fig. 3B). As $N_s$ is varied, $\gamma \propto N_s$ and $K_{sp} \propto N_s^3$. As a result, in Eq. 1, the pivoting stiffness term scales as $N_s^3$ and the tip-link force term scales as $N_s^2$, since each individual tip-link force is set by Eq. 3, of which the right-hand side is independent of $N_s$. Therefore, for small values of $N_s$, $\gamma$ is small and the combined tip-link forces, through which the calcium cycle powers the system, become small, such that the hair-bundle motion is dominated by its passive contributions. For large values of $N_s$, the pivoting-stiffness term becomes dominant, and we are driven back toward a passive behavior. As in ref. (10), we obtain characteristic frequencies that increase with the number of stereocilia $N_s$.

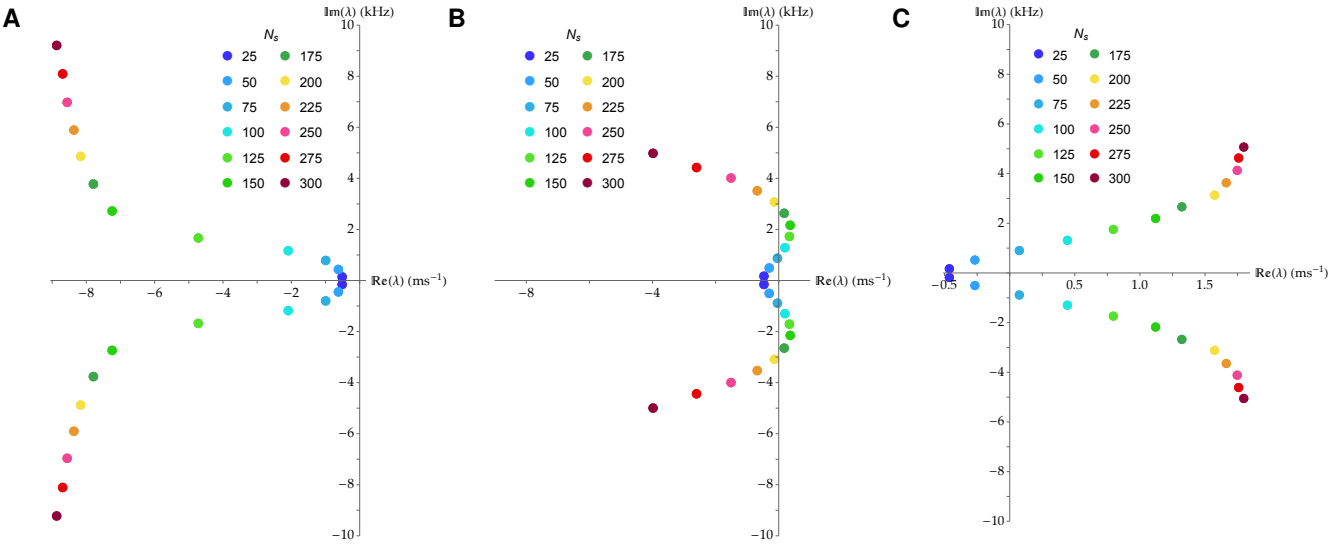


Figure 3: Dependence of the pair of eigenvalues $\lambda$ with the largest real part on the number of stereocilia $N_s$, under the constant actin-mass hypothesis and for three values of the attempt frequency $\bar{k}$. (A) For $\bar{k} = 1 \cdot 10^3\ s^{-1}$, the hair bundle displays only damped oscillations. (B) For $\bar{k} = 1 \cdot 10^4\ s^{-1}$, the hair bundle shows limit-cycle oscillations for a limited range of values of $N_s$, here roughly between 50 and 200. (C) For $\bar{k} = 5 \cdot 10^4\ s^{-1}$, the hair bundle presents limit-cycle oscillations above a threshold value of $N_s$, here around 50.

## Calcium dependency

Hair-bundle oscillations are known to be affected by the concentration of calcium in the surrounding milieu (8). In Fig. 4, we show the dependence of the eigenvalues on calcium concentration at the binding site when the channels are either open or closed, that is varying the parameters $[Ca^{2+}]^{open}$ and $[Ca^{2+}]^{closed}$, as well as on the open probability of the channels at steady state $P_{open}$. We display in Fig. 4A the dependence of the eigenvalues as a function of the number of stereocilia $N_s$, for four different values of the calcium concentration in the vicinity of the channel in the open state $[Ca^{2+}]^{open}$. We see that the system transitions from damped to limit-cycle and then back to damped oscillations as $[Ca^{2+}]^{open}$ increases, within a given range of $N_s$ values, here between 100 and 200 for $[Ca^{2+}]^{open} = 60\ \mu M$. The system displays limit-cycle oscillations for calcium concentrations in a window around 40 $\mu$M. For lower and higher values of $[Ca^{2+}]^{open}$, the eigenvalues are confined to the left of the imaginary axis, in the regime of damped oscillations, for all $N_s$ values. This can be understood from the necessity of having a cycle between the six states of Fig. 2B. At large $[Ca^{2+}]^{open}$, the system is too biased toward states 3 and 4 via the dependence of $k_{Ca}^{+,O}$ in $[Ca^{2+}]^{open}$. If $[Ca^{2+}]^{open}$ is too low, however, the opposite happens and most channels have no $Ca^{2+}$ bound. The evolution of the eigenvalues with $[Ca^{2+}]^{open}$ at fixed $N_s = 100$ is shown in Fig. 4C. We can see that the variation in characteristic frequency remains relatively small, with a slight increase toward large $[Ca^{2+}]^{open}$ values. This stems from a higher $k_{Ca}^{+,O}$ rate with larger $[Ca^{2+}]^{open}$ values.

As the impact of calcium binding on hair-bundle oscillations depends, at any given time, on the total number of open channels, we expect the behavior of the hair bundle to change as the value of the open probability at steady state is varied. In Fig. 4B, we show the eigenvalues' dependence on $N_s$ similarly to Fig. 4A, for six different values of $P_{open}$. With the parameter values given in Table 1, the hair bundle displays limit-cycle oscillations within a limited range of $P_{open}$ values, from about 0.15 to about 0.30. The existence of a range of values of $P_{open}$ for which oscillations occur can be interpreted qualitatively as follows: Varying $P_{open}$ affects the value of $\tilde{X}_0$, which sets the value of tension in the tip links via Eq. 2. This in turn affects the energies via Eq. 11, which further enter the system of equations 10 in exponential functions. The resulting steady state corresponds to relative occupancies that follow sigmoidal-type laws in the energies. If the values of these energies are too biased in a particular direction, the energy $E_{Ca}$ gained by $Ca^{2+}$ binding is not large enough to affect sufficiently the state occupancies and to power spontaneous oscillations. That illustrates why there is a range of $P_{open}$ values for which oscillations occur. In addition, this range is biased toward values of $P_{open}$ smaller than 1/2, because in the system of equations 10, not all transition rates are equally affected by the $Ca^{2+}$ binding energy $E_{Ca}$. The transitions between the open states 6, 5, and 4 are not affected by this energy $E_{Ca}$, whereas those between the closed states 1, 2, and 3 are affected by $E_{Ca}$. Therefore, the $Ca^{2+}$ binding energy is used most efficiently when the open states 6, 5, and 4 are relatively depopulated compared to states 1, 2, and 3, corresponding to an overall open probability of less than 0.5.

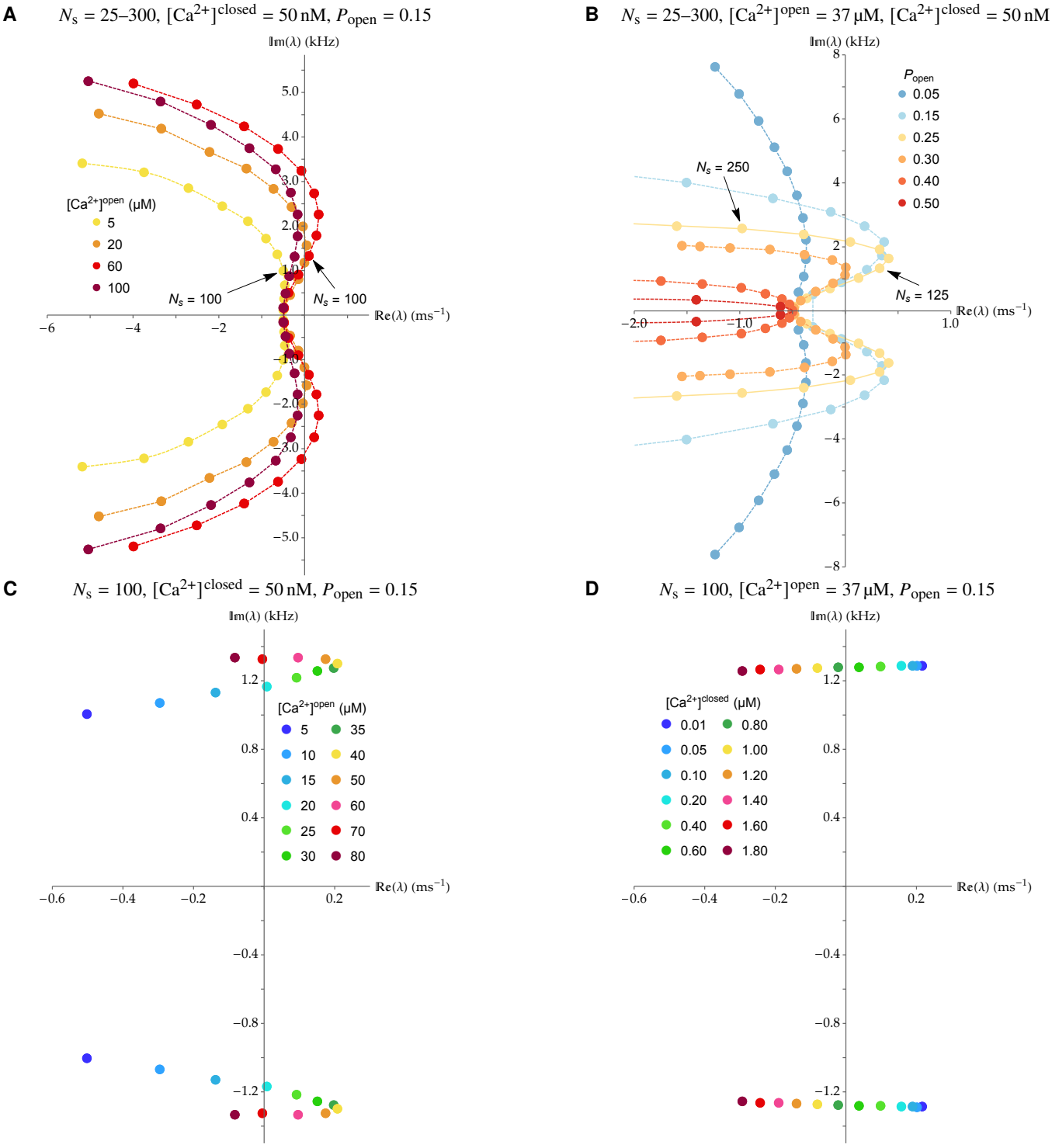


Figure 4: Dependence of the most unstable pair of eigenvalues $\lambda$ on the number of stereocilia $N_s$, the calcium concentration in the vicinity of the channel in the open state $[Ca^{2+}]^{open}$ and in the closed state $[Ca^{2+}]^{closed}$, and the open probability at rest $P_{open}$. *Top row*: (A) The eigenvalues are plotted in four families of curves, each corresponding to a different value of $[Ca^{2+}]^{open}$, while varying the number of stereocilia $N_s$ from 25 to 300 by steps of 25 as in Fig 3 and at fixed $\bar{k} = 10^4$ s$^{-1}$, $[Ca^{2+}]^{closed} = 50$ nM and $P_{open} = 0.15$. (B) The eigenvalues are plotted similarly to panel A, in six families of curves, each corresponding to a different value of $P_{open}$, for $[Ca^{2+}]^{open} = 37$ μM and with the same values of $\bar{k}$, $[Ca^{2+}]^{closed}$, and varied $N_s$ as in panel A. *Bottom row*: The eigenvalues are plotted for various calcium concentrations $[Ca^{2+}]^{open}$ (C) and $[Ca^{2+}]^{closed}$ (D) at fixed $N_s = 100$, $\bar{k} = 10^4$ s$^{-1}$, and $P_{open} = 0.15$.

In this description, we have used constant values of the local $Ca^{2+}$ concentrations $[Ca^{2+}]^{open}$ and $[Ca^{2+}]^{closed}$ in the open and closed states of the channel, respectively, which is valid only if the local $Ca^{2+}$ concentration adjusts fast enough to the channel's state. In a hemi-infinite space, the evolution of the $Ca^{2+}$ concentration a given distance from a point source, such as a mechanotransduction channel, is given by Eqs. 2.9 (when open) or 2.12 (when closed) of ref. (46), up to a factor two stemming from symmetry arguments, as in ref. (47). Hypothesizing a $Ca^{2+}$-binding site located intracellularly 5 nm away from the channel pore (10), a $Ca^{2+}$ diffusion coefficient of $8 \cdot 10^{-8}$ $m^2 \cdot s^{-1}$ (48), and with our default extracellular and intracellular steady-state $Ca^{2+}$ concentrations given in Table 1, we obtain that the $Ca^{2+}$ concentration reaches 95 % of its maximal value $[Ca^{2+}]^{open}$ only 5 µs after channel opening, to then drop within 100 µs to about 60 nM, less than 0.2 % of that value. Similar estimates are made in (10). To investigate whether this larger falling time of the $Ca^{2+}$ concentration in the closed state can have an impact on our results, we investigate in Fig. 4D the dependence of the system's eigenvalues as a function of an effective $Ca^{2+}$ concentration in the closed state, considered to be an interpolation between the different values of the local $Ca^{2+}$ concentration after the channel has closed and before it reopens, an average at the characteristic frequency of the spontaneous oscillations. We can see that the eigenvalues are hardly changed when this effective $Ca^{2+}$ concentration is varied between 10 and 100 nM, a value reached about 30 µs after channel closure. This analysis demonstrates that, to study hair-bundle oscillations up to ten kilohertz or even slightly more, we can safely ignore the rising and falling times in the local $Ca^{2+}$ concentration at the binding site and consider this to be equal to its steady-state values $[Ca^{2+}]^{open}$ and $[Ca^{2+}]^{closed}$, when the channel is in the open or closed state, respectively. As expected, increasing $[Ca^{2+}]^{closed}$ eventually causes the oscillations to cease due to $Ca^{2+}$ rebinding to the channel before it reopens Choe *et al.* (10). Moreover, since the $Ca^{2+}$ binding site is thought to be located only within several nanometers from the channel pore, $Ca^{2+}$ buffers do not play a role in the process we describe as they do not affect the $Ca^{2+}$ concentration at the binding site on the relevant timescales. The situation would change, however, if the binding site were located at significantly greater distances from the channel. Our conclusion here agrees with the results reported in (49), where it is shown that at distances from the channel shorter than the buffer 'length constant'—which for BAPTA (1,2-Bis(2-aminophenoxy)ethane-N,N,N',N'-tetraacetic acid) is about 30 nm and for EGTA (ethylene glycol-bis($\beta$-aminoethyl ether)-N,N,N',N'-tetraacetic acid) about 420 nm—the calcium concentration behaves as it would in an unbuffered scenario.

Finally, in Fig. 5, we represent the frequencies of the spontaneous oscillations, when they exist, in three dimensions as a function of the parameters $K_{sp,0}$, $N_s$, and $k_t$, at fixed $P_{open}$, $[Ca^{2+}]^{open}$, and $[Ca^{2+}]^{closed}$. Each bubble corresponds to an oscillatory state associated with a unique triplet of these parameters. Both its color and size code for the frequency of the corresponding spontaneous oscillations.

## DISCUSSION

In our previous work, we developed a new gating-spring model with cooperative channels (20) and then used it to explain changes observed in the biophysical properties of hair cells during development and tip-link regeneration (50). In the present paper, we have developed the model further and shown how the mechanotransduction apparatus of a hair cell can not only transduce, but also amplify incident sounds at kilohertz frequencies, typical of amniote hearing. Specifically, we have investigated whether, within this framework, the electrochemical gradient of $Ca^{2+}$ can power spontaneous oscillations in hair cells at such frequencies.

The proposal that the electrochemical gradient of $Ca^{2+}$ ions can power the active process through their binding and unbinding to the mechanosensitive channels is not new. Our work was particularly influenced by that of Choe *et al.* (10) showing that a Hopf bifurcation can arise from the $Ca^{2+}$-dependent fast adaptation mechanism, without the need for myosin-motor activity. There are, however, major differences between the two models. In the work by Choe *et al.*, all the 'forward' rate constants were identical, as were their symmetric 'reverse' rate constants. Taking different values for these two rate constants therefore drove the cycle of hair-bundle oscillations. Here, instead, the rate constants are based on Kramers' rate theory, using the OC state of the channel pair as the activation state. The oscillations are driven by the electrochemical gradient of $Ca^{2+}$, as described by the out-of-equilibrium rates of $Ca^{2+}$ binding and unbinding in Eq. 6. The second main difference is that here a single calcium binding site per channel suffices to give rise to spontaneous oscillations, whereas two binding sites were required in the work by Choe *et al.* for energetic and kinetic considerations. Finally, due to the mobility of the channels within the lipid membrane, together with a difference in membrane elastic energies between the OO and CC states of the channel pair, our model is capable of producing spontaneous oscillations without requiring a large individual-channel gating swing. It relies instead chiefly on the state-dependent changes in the thickness of the hydrophobic core of the channel at the interface with the lipid bilayer, resulting in the mutual attraction or repulsion of the channels at short distances (20, 21, 30).

Our results are consistent with a number of experimental findings: First, the frequency of spontaneous oscillations increases with the number of stereocilia, in agreement with the tonotopic arrangement along the cochlea (44, 45). Second, Tobin *et al.* showed that all three parameters, $N_s$, $k_t$ and $K_{sp}$ increase their values along the tonotopic axis of the cochlea (44). This is in agreement with the results shown in Fig. 5, where the characteristic frequency of oscillations increases as these parameters are simultaneously increased. Third, spontaneous oscillations in the model arise only in a limited range of $Ca^{2+}$ concentration. With

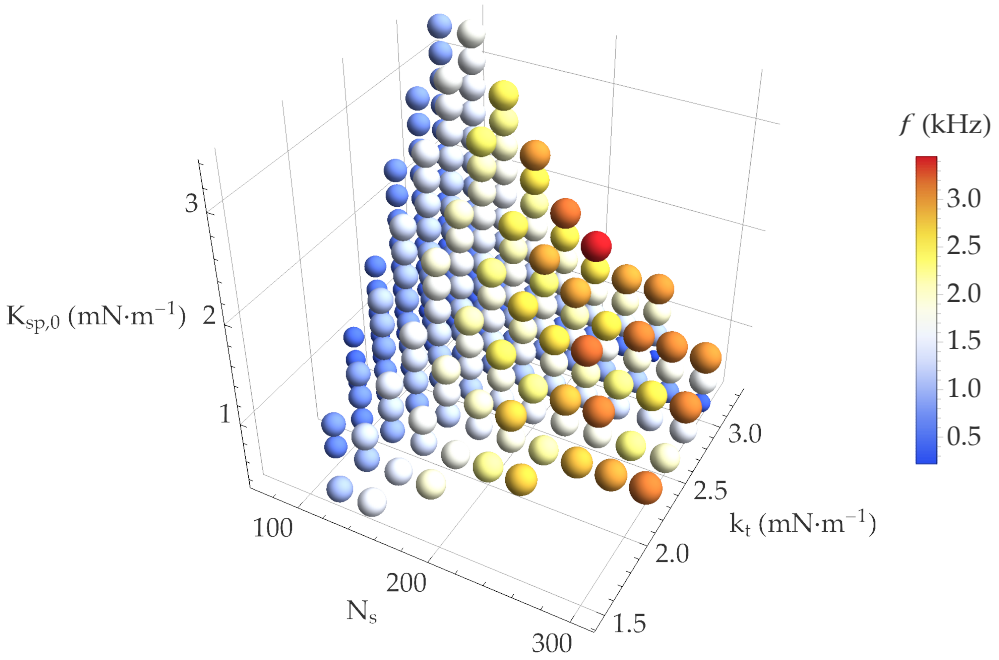


Figure 5: 4D plot of the parameter values for which the system shows limit-cycle oscillations as a function of $k_t$, $N_s$ and $K_{sp,0}$, with $\bar{k} = 10^4$ s$^{-1}$, $P_{open} = 0.15$, $[Ca^{2+}]^{open} = 37\,\mu M$, and $[Ca^{2+}]^{closed} = 50$ nM. Each plotted bubble corresponds to an oscillatory state. As the corresponding frequency varies from 0.2 kHz to 3.5 kHz, the color of the bubbles changes from blue to red and their size increases.

physiological parameters, this range is approximately 20–70 $\mu$M, in agreement with the $Ca^{2+}$ concentration of the cochlear endolymph (51). The results show a similar trend as a function of the open probability at rest, for which we observe spontaneous oscillations between approximately 0.10 and 0.35. This range corresponds to the open probabilities of the mechanotransduction channels in mammalian inner hair cells as well as in hair cells of some lizard species (38, 39, 52). Therefore, given the shape of the sigmoidal open-probability vs. displacement curve, a high-frequency sinusoidal stimulus results in a non-zero integral voltage response at such open probabilities (38). We conclude from these results that the range of resting open probabilities characteristic of these hair cells not only maximizes the integrated voltage response for a given high-frequency input but is also compatible with mechanical amplification.

In the experimentally observed and extensively modeled low-frequency oscillations of hair cells from the bullfrog sacculus, the myosin motors play a direct role in the oscillations (53, 54). The hair-bundle negative stiffness and the motor-based slow adaptation together engender large-amplitude oscillations in those vestibular hair cells tuned to frequencies of several hertz to tens of hertz (8, 53). During a complete cycle of these relaxation oscillations, the channels' open probability varies extensively, from almost zero to about one. In contrast, myosin motors do not play a direct role in the amplification mechanism proposed here. Instead, their role is implicitly limited to setting the channels' open probability at steady state to a specific value, which they are known to do by means of a process called 'slow adaptation' (4, 55). Our results indicate that large-amplitude oscillations are neither expected from the proposed amplification mechanism nor required to support the active process in general. Sufficiently close to the instability threshold of a supercritical Hopf bifurcation, the oscillation amplitude is arbitrarily small and the open probability can remain near its target value at all times. This could be the reason why, experimentally, one has never observed spontaneous oscillations in cochlear hair cells tuned to frequencies in the kilohertz range. It is possible that spontaneous oscillations in these cells remain so small that they are practically unobservable due to Brownian motion and measurement noise. Therefore, despite the absence of any direct experimental evidence so far, it is possible that auditory hair cells act as cochlear amplifiers at kilohertz frequencies through the mechanism described in this study.

## AUTHOR CONTRIBUTIONS

A.K. conceived and designed the project; T.R. and A.K. directed the project; E.D. and T.R. designed the model; F.G., B.H., E.D., and T.R. wrote the code; F.G. produced the results and the figures; F.G., T.R., and A.K. interpreted the results and wrote the paper. A.K. and T.R. contributed equally to this project.

## DECLARATION OF INTERESTS

The authors declare no competing interests.

## ACKNOWLEDGMENTS

Work on this project in the Kozlov lab was funded by the Wellcome Trust (108034/Z/15/Z and 214234/Z/18/Z) and the Imperial College Network of Excellence Award. This work received support from the grants ANR-11-LABX-0038, ANR-10-IDEX-0001-02.

## REFERENCES

1. Gold, T., 1948. Hearing. II. The Physical Basis of the Action of the Cochlea. *Proceedings of the Royal Society of London B: Biological Sciences* 135:492–498.

2. Hudspeth, A. J., 2008. Making an Effort to Listen: Mechanical Amplification in the Ear. *Neuron* 59:530–545.

3. Hudspeth, A. J., Y. Choe, A. D. Mehta, and P. Martin, 2000. Putting Ion Channels to Work: Mechanoelectrical Transduction, Adaptation, and Amplification by Hair Cells. *Proceedings of the National Academy of Sciences* 97:11765–11772.

4. Fettiplace, R., and K. X. Kim, 2014. The Physiology of Mechanoelectrical Transduction Channels in Hearing. *Physiological Reviews* 94:951–986.

5. Hudspeth, A. J., F. Jülicher, and P. Martin, 2010. A Critique of the Critical Cochlea: Hopf—a Bifurcation—Is Better Than None. *Journal of Neurophysiology* 104:1219–1229.

6. Strogatz, S. H., 2018. Nonlinear Dynamics and Chaos with Student Solutions Manual: With Applications to Physics, Biology, Chemistry, and Engineering, Second Edition. CRC Press.

7. Kemp, D. T., 1978. Stimulated Acoustic Emissions from within the Human Auditory System. *The Journal of the Acoustical Society of America* 64:1386–1391.

8. Martin, P., D. Bozovic, Y. Choe, and A. J. Hudspeth, 2003. Spontaneous Oscillation by Hair Bundles of the Bullfrog's Sacculus. *Journal of Neuroscience* 23:4533–4548.

9. Tinevez, J.-Y., F. Jülicher, and P. Martin, 2007. Unifying the Various Incarnations of Active Hair-Bundle Motility by the Vertebrate Hair Cell. *Biophysical Journal* 93:4053–4067.

10. Choe, Y., M. O. Magnasco, and A. J. Hudspeth, 1998. A Model for Amplification of Hair-Bundle Motion by Cyclical Binding of Ca2+ to Mechanoelectrical-Transduction Channels. *Proceedings of the National Academy of Sciences* 95:15321–15326.

11. Nam, J.-H., and R. Fettiplace, 2008. Theoretical Conditions for High-Frequency Hair Bundle Oscillations in Auditory Hair Cells. *Biophysical Journal* 95:4948–4962.

12. Meenderink, S. W. F., P. M. Quiñones, and D. Bozovic, 2015. Voltage-Mediated Control of Spontaneous Bundle Oscillations in Saccular Hair Cells. *Journal of Neuroscience* 35:14457–14466.

13. Ricci, A. J., A. C. Crawford, and R. Fettiplace, 2002. Mechanisms of Active Hair Bundle Motion in Auditory Hair Cells. *Journal of Neuroscience* 22:44–52.

14. Kennedy, H. J., A. C. Crawford, and R. Fettiplace, 2005. Force Generation by Mammalian Hair Bundles Supports a Role in Cochlear Amplification. *Nature* 433:880–883.

15. Ashmore, J., 2019. Outer Hair Cells and Electromotility. *Cold Spring Harbor Perspectives in Medicine* 9:a033522.

16. Santos-Sacchi, J., and W. Tan, 2019. Voltage Does Not Drive Prestin (SLC26a5) Electro-Mechanical Activity at High Frequencies Where Cochlear Amplification Is Best. *iScience* 22:392–399.

17. Vavakou, A., N. P. Cooper, and M. van der Heijden, 2019. The Frequency Limit of Outer Hair Cell Motility Measured in Vivo. *eLife* 8:e47667.

18. Santos-Sacchi, J., 1991. Reversible Inhibition of Voltage-Dependent Outer Hair Cell Motility and Capacitance. *Journal of Neuroscience* 11:3096–3110.

19. Chan, D. K., and A. J. Hudspeth, 2005. Ca2+ Current–Driven Nonlinear Amplification by the Mammalian Cochlea in Vitro. *Nature Neuroscience* 8:149–155.

20. Gianoli, F., T. Risler, and A. S. Kozlov, 2017. Lipid Bilayer Mediates Ion-Channel Cooperativity in a Model of Hair-Cell Mechanotransduction. *Proceedings of the National Academy of Sciences* 114:E11010–E11019.

21. Ursell, T., K. C. Huang, E. Peterson, and R. Phillips, 2007. Cooperative Gating and Spatial Organization of Membrane Proteins through Elastic Interactions. *PLOS Computational Biology* 3:e81.

22. Beurg, M., M. G. Evans, C. M. Hackney, and R. Fettiplace, 2006. A Large-Conductance Calcium-Selective Mechanotransducer Channel in Mammalian Cochlear Hair Cells. *Journal of Neuroscience* 26:10992–11000.

23. Beurg, M., R. Fettiplace, J.-H. Nam, and A. J. Ricci, 2009. Localization of Inner Hair Cell Mechanotransducer Channels Using High-Speed Calcium Imaging. *Nature Neuroscience* 12:553–558.

24. Kachar, B., M. Parakkal, M. Kurc, Y.-d. Zhao, and P. G. Gillespie, 2000. High-Resolution Structure of Hair-Cell Tip Links. *Proceedings of the National Academy of Sciences* 97:13336–13341.

25. Tang, Y.-Q., S. A. Lee, M. Rahman, S. A. Vanapalli, H. Lu, and W. R. Schafer, 2020. Ankyrin Is An Intracellular Tether for TMC Mechanotransduction Channels. *Neuron* 107:112–125.e10.

26. Kurima, K., L. M. Peters, Y. Yang, S. Riazuddin, Z. M. Ahmed, S. Naz, D. Arnaud, S. Drury, J. Mo, T. Makishima, M. Ghosh, P. S. N. Menon, D. Deshmukh, C. Oddoux, H. Ostrer, S. Khan, S. Riazuddin, P. L. Deininger, L. L. Hampton, S. L. Sullivan, J. F. Battey, B. J. B. Keats, E. R. Wilcox, T. B. Friedman, and A. J. Griffith, 2002. Dominant and Recessive Deafness Caused by Mutations of a Novel Gene, TMC1, Required for Cochlear Hair-Cell Function. *Nature Genetics* 30:277–284.

27. Pan, B., G. S. G. Géléoc, Y. Asai, G. C. Horwitz, K. Kurima, K. Ishikawa, Y. Kawashima, A. J. Griffith, and J. R. Holt, 2013. TMC1 and TMC2 Are Components of the Mechanotransduction Channel in Hair Cells of the Mammalian Inner Ear. *Neuron* 79:504–515.

28. Pan, B., N. Akyuz, X.-P. Liu, Y. Asai, C. Nist-Lund, K. Kurima, B. H. Derfler, B. György, W. Limapichat, S. Walujkar, L. N. Wimalasena, M. Sotomayor, D. P. Corey, and J. R. Holt, 2018. TMC1 Forms the Pore of Mechanosensory Transduction Channels in Vertebrate Inner Ear Hair Cells. *Neuron* 99:736–753.e6.

29. Nielsen, C., M. Goulian, and O. S. Andersen, 1998. Energetics of Inclusion-Induced Bilayer Deformations. *Biophysical Journal* 74:1966–1983.

30. Phillips, R., T. Ursell, P. Wiggins, and P. Sens, 2009. Emerging Roles for Lipids in Shaping Membrane-Protein Function. *Nature* 459:379–385.

31. Howard, J., and A. J. Hudspeth, 1988. Compliance of the Hair Bundle Associated with Gating of Mechanoelectrical Transduction Channels in the Bullfrog's Saccular Hair Cell. *Neuron* 1:189–199.

32. Baumgart, J., 2011. The Hair Bundle: Fluid-Structure Interaction in the Inner Ear. Ph.D. thesis.

33. Assad, J. A., and D. P. Corey, 1992. An Active Motor Model for Adaptation by Vertebrate Hair Cells. *Journal of Neuroscience* 12:3291–3309.

34. Jaramillo, F., and A. J. Hudspeth, 1993. Displacement-Clamp Measurement of the Forces Exerted by Gating Springs in the Hair Bundle. *Proceedings of the National Academy of Sciences* 90:1330–1334.

35. Beurg, M., J.-H. Nam, A. Crawford, and R. Fettiplace, 2008. The Actions of Calcium on Hair Bundle Mechanics in Mammalian Cochlear Hair Cells. *Biophysical Journal* 94:2639–2653.

36. Russell, I. J., and P. M. Sellick, 1983. Low-Frequency Characteristics of Intracellularly Recorded Receptor Potentials in Guinea-Pig Cochlear Hair Cells. *The Journal of Physiology* 338:179–206.

37. Russell, I. J., and M. Kössl, 1991. The Voltage Responses of Hair Cells in the Basal Turn of the Guinea-Pig Cochlea. *The Journal of Physiology* 435:493–511.

38. Chiappe, M. E., A. S. Kozlov, and A. J. Hudspeth, 2007. The Structural and Functional Differentiation of Hair Cells in a Lizard's Basilar Papilla Suggests an Operational Principle of Amniote Cochleas. *Journal of Neuroscience* 27:11978–11985.

39. Johnson, S. L., 2015. Membrane Properties Specialize Mammalian Inner Hair Cells for Frequency or Intensity Encoding. *eLife* 4:e08177.

40. Zhang, T.-Y., S. Ji, and D. Bozovic, 2015. Synchronization of Spontaneous Active Motility of Hair Cell Bundles. *PLOS ONE* 10:e0141764.

41. Kozlov, A. S., J. Baumgart, T. Risler, C. P. C. Versteegh, and A. J. Hudspeth, 2011. Forces between Clustered Stereocilia Minimize Friction in the Ear on a Subnanometre Scale. *Nature* 474:376–379.

42. Flock, Å., and D. Strelioff, 1984. Graded and Nonlinear Mechanical Properties of Sensory Hairs in the Mammalian Hearing Organ. *Nature* 310:597–599.

43. Tilney, L. G., and J. C. Saunders, 1983. Actin Filaments, Stereocilia, and Hair Cells of the Bird Cochlea. I. Length, Number, Width, and Distribution of Stereocilia of Each Hair Cell Are Related to the Position of the Hair Cell on the Cochlea. *Journal of Cell Biology* 96:807–821.

44. Tobin, M., A. Chaiyasitdhi, V. Michel, N. Michalski, and P. Martin, 2019. Stiffness and Tension Gradients of the Hair Cell's Tip-Link Complex in the Mammalian Cochlea. *eLife* 8:e43473.

45. Tilney, L. G., and M. S. Tilney, 1988. The Actin Filament Content of Hair Cells of the Bird Cochlea Is Nearly Constant Even Though the Length, Width, and Number of Stereocilia Vary Depending on the Hair Cell Location. *The Journal of Cell Biology* 107:2563–2574.

46. Berg, H. C., 1993. Random Walks in Biology: Expanded Edition. Princeton University Press.

47. Lumpkin, E. A., and A. J. Hudspeth, 1998. Regulation of Free Ca2+ Concentration in Hair-Cell Stereocilia. *Journal of Neuroscience* 18:6300–6318.

48. Hille, B., 1992. Ionic Channels of Excitable Membranes. Sinauer Associates, Sunderland, Mass.

49. Naraghi, M., and E. Neher, 1997. Linearized Buffered Ca2+ Diffusion in Microdomains and Its Implications for Calculation of [Ca2+] at the Mouth of a Calcium Channel. *Journal of Neuroscience* 17:6961–6973.

50. Gianoli, F., T. Risler, and A. S. Kozlov, 2019. The Development of Cooperative Channels Explains the Maturation of Hair Cell's Mechanotransduction. *Biophysical Journal* 117:1536–1548.

51. Bosher, S. K., and R. L. Warren, 1978. Very Low Calcium Content of Cochlear Endolymph, an Extracellular Fluid. *Nature* 273:377–378.

52. Manley, G. A., U. Sienknecht, and C. Köppl, 2004. Calcium Modulates the Frequency and Amplitude of Spontaneous Otoacoustic Emissions in the Bobtail Skink. *Journal of Neurophysiology* 92:2685–2693.

53. Martin, P., A. D. Mehta, and A. J. Hudspeth, 2000. Negative Hair-Bundle Stiffness Betrays a Mechanism for Mechanical Amplification by the Hair Cell. *Proceedings of the National Academy of Sciences* 97:12026–12031.

54. Le Goff, L., D. Bozovic, and A. J. Hudspeth, 2005. Adaptive Shift in the Domain of Negative Stiffness during Spontaneous Oscillation by Hair Bundles from the Internal Ear. *Proceedings of the National Academy of Sciences of the United States of America* 102:16996–17001.

55. Holt, J. R., and D. P. Corey, 2000. Two Mechanisms for Transducer Adaptation in Vertebrate Hair Cells. *Proceedings of the National Academy of Sciences* 97:11730–11735.